Borrell Tomás, MA.; Salvador Moya, MD.; Garcia-Rocha, V.; Fernandez, A.; Chicardi, E.; Gotor, FJ. (2012). Spark plasma sintering of TiyNb1-yCxN1-x monolithic ceramics obtained by mechanically induced self-sustaining reaction. Materials Science and Engineering: A. 543:173-179. doi:10.1016/j.msea.2012.02.071.

Spark plasma sintering of $Ti_yNb_{1-y}C_xN_{1-x}$ monolithic ceramics obtained by mechanically induced self-sustaining reaction

Amparo Borrell*[1,2], María Dolores Salvador[1], Victoria García-Rocha[3], Adolfo Fernández[2,3], Ernesto Chicardi[4], Francisco J. Gotor[4]

[1]Instituto de Tecnología de Materiales (ITM), Universidad Politécnica de Valencia, Camino de Vera s/n, 46022 Valencia, Spain

[2]Centro de Investigación en Nanomateriales y Nanotecnología (CINN) (Consejo Superior de Investigaciones Científicas - Universidad de Oviedo - Principado de Asturias), Parque Tecnológico de Asturias, 33428 Llanera (Asturias), Spain

[3]ITMA Materials Technology, Parque Tecnológico de Asturias, 33428 Llanera (Asturias), Spain

[4]Instituto de Ciencia de Materiales de Sevilla (CSIC-US), Calle Américo Vespucio 49, 41092 Sevilla, Spain

[*] Corresponding author at: Instituto de Tecnología de Materiales (ITM), Universidad Politécnica de Valencia, Camino de Vera s/n, 46022 Valencia, Spain

Tel.: +34 (963) 877 007; Fax: +34 (963) 877 629

E-mail address: aborrell@upvnet.upv.es (A. Borrell)

ABSTRACT

Nanometer-sized titanium-niobium carbonitride powders ($Ti_yNb_{1-y}C_xN_{1-x}$) with different Ti/Nb atomic ratios were obtained by a mechanically induced self-sustaining

reaction, and sintered by spark plasma sintering technique at 1500 ºC for 1 min in a vacuum atmosphere. Mechanical properties such as hardness and Young's modulus were determined by nanoindentation technique and friction and wear coefficients assessed by ball-on-disk testing using alumina ball in dry sliding conditions. The fracture surface and wear tracks of samples were examined by scanning electron microscopy. Results showed that it is possible to obtain dense monolithic ceramics from the solid solution ($Ti_yNb_{1-y}C_xN_{1-x}$) with good mechanical properties and excellent wear resistance. The optimum values of nanomechanical properties were found for the $Ti_{0.3}Nb_{0.7}C_{0.5}N_{0.5}$ ceramic composition, which exhibited a high hardness over 26.0 GPa and Young's modulus around 400 GPa.

Keywords: TiNbCN; Spark Plasma Sintering; Microstructure; Mechanical properties; Wear resistance

1. Introduction

Transition metal carbonitrides are becoming increasingly important materials for their excellent properties in the fields of superhardness, tribology, superconductivity and, electrical and thermal conductivities [1]. Titanium carbonitride is the most widely employed material because it is the main component in commercial cermets. These cermets are prepared from a Ti(C, N) powder, or a combination of TiC and TiN powders, with Ni as binder and are manufactured by sintering the compacted powder mixture at a temperature at which a liquid phase is formed [2,3]. To produce Ti(C, N)-based cermets, the most commonly used production routes are hot pressing (HP), hot isostatic pressing (HIP'ing), or a combination of HIP'ing and sintering, under vacuum,

nitrogen or argon atmosphere. One of the most common ways to prepare titanium carbonitride is to hot press blended mixtures of TiC and TiN powders in vacuum or argon atmosphere at 1700-2400 ºC [4-7]. More recently, the spark plasma sintering (SPS) method has emerged as a useful technology and has already been used to densify titanium carbonitride powders at a relatively low temperature. This technique can work at heating rates of the order of hundreds of degrees per minute, reaching high temperatures in very short time, leading to dense materials after cycles of heating/cooling in the order of a few minutes compared to conventional methods [8,9].

The physical and mechanical properties of Ti(C, N)-based cermets can be adjusted to meet the specific requirements of cutting tasks by adding a variety of binary carbides such as WC, TaC, NbC, and Mo_2C [10]. In these cermets, the typical core-rim structure is developed for the hard phase during the liquid phase sintering, being the core the original undisolved Ti(C,N) particle and the rim a newly formed complex carbonitride solid solution [11]. Good cutting performance of cermets is attributable to the mechanical behaviour of this rim phase and, therefore, many studies have focussed on changing the composition of this mixed carbonitride [12]. Moreover, bimetallic nitrides have also shown better performances than single metal nitrides and allow a better control of the mechanical and electronic properties. Recently, many ternary metal nitrides have been reported [13-15]. However, these researches mostly focused on thin films, coatings and powders, but few reports concerned bulk materials.

The possibility of employing this type of complex solid solutions in the development of new materials would permit the opening of innovative ways to optimize the set of properties that must be targeted for specific technological applications. However, so far, appropriate methods for synthesizing them in a proper and reproducible way have not been developed yet. Recently, Córdoba et al. [16,17] have

shown that the mechanochemical process denoted as a mechanically induced self-sustaining reaction (MSR) can be considered as an alternative technique to be used in the synthesis of complex carbonitride phases. This reactive milling method uses the strong exothermic character of the formation of carbonitrides from the elements to be obtained with high purity and good control of stoichiometry.

In a previous work [9], TiC_xN_{1-x} powders obtained by MSR were successfully densified by SPS, so that the main mechanical properties of the final ceramic material could be evaluated. In this work, the promising procedure of coupling MSR and SPS techniques was employed to obtain completely dense $Ti_yNb_{1-y}C_xN_{1-x}$ monolithic ceramics and the mechanical and wear properties of the solid solution were studied as a function of the Ti and Nb contents.

2. Experimental procedure

Titanium powder (99% in purity, <325 mesh, Strem Chemicals, Newburyport, MA, USA), niobium powder (99.8% in purity, <60 mesh, Aldrich, Milwaukee, WI, USA) and graphite powder (11 m^2 g^{-1}, Fe ≤ 0.4%, Merck, Whitehouse Station, NJ, USA) were used in this work. 46.5 g of different powder mixtures of titanium, niobium, and graphite together with fifteen tempered steel balls (d = 20 mm, m = 32.6 g) were placed in a 300 ml tempered steel vial (67Rc) and milled under 6 atm of high-purity nitrogen gas (H_2O and O_2 ≤3 ppm, Air Liquide, Paris, France) using a modified planetary ball mill (Vario-Planetary Mill Pulverisette 4, Fritsch, Idar-Oberstein, Germany). The powder-to-ball mass ratio (PBR) was ~1/10.5 and a spinning rate of 400 rpm for both the rotation of the supporting disc and the superimposed rotation in the direction opposite to the vial was employed. The vial was purged with nitrogen gas

several times, and afterward the desired nitrogen pressure (6 atm) was selected before milling. The planetary mill allowed operation at a constant gas pressure and the detection of self-propagating reactions during milling. This was possible by connecting the vial to a gas cylinder via a rotating union (model 1005-163-038, Deublin, Waukegan, IL, USA) and a flexible polyamide tube, and monitoring continuously the gas pressure with an SMC solenoid valve (model EVT307-5DO-01F-Q, SMC Co., Tokyo, Japan) connected to a data acquisition system (ADAM-4000 series, Esis Pty Ltd., Pennant Hills, Australia). When the self-sustaining reaction takes place, the increasing temperature due to the exothermic reaction produces an instantaneous increase in the total pressure inside the vial, and ignition time can be obtained from the spike observed in the time-pressure record.

Powder samples obtained by MSR were sintered using an SPS apparatus HP D 25/1 (FCT Systeme GmbH, Rauenstein, Germany) at a final temperature of 1500 ºC and 80 MPa of pressure to obtain fully sintered bulk materials. In each test, 5 g of material were used, which were introduced into a 20-mm-diameter graphite die. The tests were carried out under vacuum at a heating rate of 100 ºC min^{-1} with a 1-min dwelling time at the maximum temperature. The density was measured by the Archimedes method (ISO-3369). The final relative densities were estimated in accordance with the rule of mixtures. Six specimens were evaluated for each composition.

X-ray diffraction (XRD) diagrams of powders and polished surfaces of dense ceramics were performed using a Philips X'Pert Pro instrument (Amsterdam, the Netherlands) equipped with a Θ/Θ goniometer using CuKa radiation (40 kV, 40 mA), a secondary K_β filter, and an X'Celerator detector. The diffraction diagrams were scanned from 20º to 140º (2θ) in step-scan mode at a step of 0.02º and a counting time of 275 s/step. The Rietveld refinement method was employed for the lattice parameter

determination and the quantitative phase analysis of products by using the freely distributed Fullprof computer program [18].

Nanomechanical properties such as Young's modulus and hardness of samples were obtained by nanoindentation technique (Model G200, MTS Company, USA). To carry out indentations at very low depths, a brand new Berkovich diamond tip was used with radius less than 20 nm as certified by the manufacturing company. In order to ensure the quality of the tip throughout the work, pre- and post- calibration procedures were performed for this indenter ensuring the correct calibration of its function area and correct machine compliance. Previous to the nanoindenter testing, the samples were prepared by metallographic techniques. After cutting, the surface was lapped and then polished, with a final step with 0.25 µm diamond paste, giving a surface roughness in the nanometer range. The nanomechanical properties of the $Ti_yNb_{1-y}C_xN_{1-x}$ ceramics were evaluated from the load-displacement nanoindentation data using the widely accepted Oliver and Pharr method [19].

Reduced Young's modulus, E^*, was estimated according to the following equation:

$$E^* = \frac{1}{2}\sqrt{\frac{\Pi}{A(hc)}}\left|\frac{dP}{dh}\right|_{h=h\max} \qquad (1)$$

where $A(hc)$ stands the contact area which is calculated from the contact of depth hc and with the reached depth penetration $hmax$ for a Berkovich tip geometry. Young's modulus E, which is material constant, was derived from reduced Young's modulus E^* using the well known Hertzian equation:

$$\frac{1}{E^*} = \frac{1-\nu^2}{E} + \frac{1-\nu'^2}{E'} \qquad (2)$$

For this calculation, the Poisson's ratio υ'^{2} and elastic modulus E' of the diamond indenter, are 0.07 and 1141 GPa, respectively. We calculate the Young's modulus using a Poisson's ratio = 0.18. This value is chosen assuming Poisson's ratio of the phases: u = 0.17 for TiC, u = 0.19 for TiN, and u = 0.182 for TiCN [20,21]. Hardness is calculated by the quotient of *Pmax* and contact area:

$$H = \frac{P\max}{A(hc)} \tag{3}$$

The fracture toughness (K_{IC}) was measured by the indentation method under indentation load of 306 N using the expression derived by Shetty et al. [22]:

$$H_{IC} = 0.178H^{1/2}\left(\frac{P}{l}\right)^{1/2} \tag{4}$$

where H is the hardness, P is the applied load and l is the crack length at the surface. There have been 10 indentations per sample, evenly distributed, to obtain a representative toughness value of material.

Wear tests were carried out under dry sliding conditions using a tribometer ball-on-disk according to ASTM wear testing standard G99-03. As friction partners, alumina balls 5 mm in diameter were used. The sample surfaces were polished with 1 micron diamond slurry. The normal load, sliding speed and distance were fixed at 20 N, 250 rpm and 1000 m, respectively. Testing was carried out in air and at room temperature. The friction coefficient was taken as an average over the final part of the curve after the initial period of stabilization. The specific wear rates of the cermets were estimated as the worn volume/unit load and sliding distance ($mm^3\ N^{-1}\ m^{-1}$). The damage was studied on the worn surfaces of disks using scanning electron microscopy (SEM, Zeiss DSM 950, Oberchen, Germany).

3. Results and discussions

3.1. Synthesis and sintering of $Ti_yNb_{1-y}C_xN_{1-x}$

Five different mixtures containing titanium and/or niobium, and graphite powders were ball milled under a nitrogen atmosphere in order to get through a MSR process solid solution phases belonging to the Ti(C,N)-Nb(C,N) system. The relative amount of carbon was held constant and only the Ti/Nb ratio was varied (Table 1). The samples were labelled according to the nominal composition of titanium and niobium, and the prefix P refers to their powdery nature. For all of the mixtures, the time-pressure record, monitored during milling, confirmed the appearance of self-sustaining reactions, and the corresponding ignition times (t_{ig}) are shown in Table 1. After ignition, milling was prolonged for 30 min in order to ensure maximum conversion and obtain a homogeneous product. The high local temperatures reached during a MSR process provoke the formation of quite large aggregates and the post-combustion milling is a necessary step to crush these aggregates and homogenize the entire sample for the subsequent sintering process.

Figure 1 shows the XRD diagrams of products obtained after the MSR process, which revealed that the reactants were converted into a cubic phase with *Fm-3m* space group, as confirmed with DICVOL06 powder indexing software [23]. By comparison with the reference diffraction patterns corresponding to the binary compounds NbC (38-1364), NbN (38-1155), TiC (32-1383), and TiN (38-1420), these cubic phases were assigned to a complex titanium-niobium carbonitride solid solution that can be described by the general equation $Ti_yNb_{1-y}C_xN_{1-x}$. This can be easily seen in Figure

1(ii), which shows how the (200) XRD reflection of the obtained products were between the reflections corresponding to niobium and titanium nitrides and carbides. On the other hand, in samples containing niobium, the presence of a small amount of unreacted Nb was detected. In samples P-T3N7 and P-N1, the existence of Nb_2C was also observed as a minor phase. The phase quantification from the Rietveld refinement confirmed that the amount of unreacted Nb never exceeded 6 wt.% and the highest content of Nb_2C was found in sample P-N1 with 14 wt.%.

The shift observed in the XRD reflections (see the (200) reflection in Figure 1(ii)) was the result of different stoichiometry in the solid solutions, in particular different *y* values (Ti/Nb atomic ratio), which induced changes in the lattice parameter of the cubic structure. Using the FULLPROF program, the lattice parameter, *a*, was calculated from the whole XRD diagram (30-140º), and the values are shown in Table 1. Drawing on previous studies dealing with the synthesis of TiC_xN_{1-x} and NbC_xN_{1-x} powders by the same procedure [24,25], the lattice parameters for P-T1 and P-N1 samples were close to the expected values for $TiC_{0.5}N_{0.5}$ and $NbC_{0.5}N_{0.5}$, respectively. Moreover, the lattice parameters of the quaternary phases (samples P-T7N3, P-T5N5, and P-T3N7) were between the aforementioned values, confirming the formation of a $TiC_{0.5}N_{0.5}$-$NbC_{0.5}N_{0.5}$ solid solution. Finally, the significant line broadening of reflections in Figure 1 as well as previous results in similar systems [24,25] suggested the nanometer character of the obtained solid solution.

The $Ti_yNb_{1-y}C_xN_{1-x}$ powders were consolidated by spark plasma sintering technique at 1500 ºC and 80 MPa of pressure with a 1-min dwelling time at the maximum temperature. Densities of the monolithic ceramics, which were labeled with the prefix **C** to refer to their consolidated nature, are presented in Table 2. It can be seen as the absolute density of ceramics increased with the niobium content from 5.81 to

7.77 g cm^{-3}. High relative density values (>98.7%) were achieved for all the samples being the relative density of quaternary ceramics (specimens C-T7N3, C-T5N5, and C-T3N7) slightly higher than that of the ternary end-members of the solid solution.

Figure 2 shows the XRD diagrams of the monolithic ceramics after the SPS process. The reflections corresponding to the $Ti_yNb_{1-y}C_xN_{1-x}$ solid solution are clearly visible. In Figure 2ii, the shift of the (200) reflection due to a different Ti/Nb ratio in the ceramic phase is observed. A striking finding was the fact that unreacted Nb and secondary Nb_2C phase observed in some of the powder samples were not detected after sintering; suggesting that during SPS process the completion of the transformation of the reactants into the desired $Ti_yNb_{1-y}C_xN_{1-x}$ phase was achieved. The incorporation of this small amount of unreacted Nb into the solid solution structure produced only a slight variation of the lattice parameter, which is also shown in Table 2.

In Figure 3 the dependence of the lattice parameter of $Ti_yNb_{1-y}C_xN_{1-x}$ on the starting nominal composition is plotted and it shows good linearity. From these experimental results it can be concluded that the chemical composition of the solid solution in the consolidated ceramic is similar to the solid solution obtained by MSR process. The chemical composition of dense ceramics can be tailored by simple adjustment of the stoichiometry in the starting mixture.

A careful examination of Figure 2 revealed that the XRD diagrams of the quaternary ceramics (specimens C-T7N3, C-T5N5, and C-T3N7) featured broader reflections than C-T1 and C-N1 ceramics. This observation indicated that the presence of both elements Nb and Ti in the carbonitride structure reduced the grain growth of

ceramic particles during the SPS process as confirmed from the fracture surfaces that will be shown later (Figure 5). This fact can also account for the higher density observed in these samples.

3.2. Mechanical properties

The nanomechanical properties of ceramics are shown in Figure 4. All the ceramic materials showed high hardness, and quaternary ceramics exhibited enhanced values when compared with C-T1 and C-N1 specimens. The hardness values increased continuously with increasing niobium percentage, reaching a maximum value for the $Ti_{0.3}Nb_{0.7}C_{0.5}N_{0.5}$ composition (26.0 GPa). This sample also showed the highest Young's module value (400 GPa), although variation of this parameter with the composition was less pronounced. Despite there are no reference values in the literature for these complex ceramic materials, the hardness values reported of some binary compounds show that they are of the order of magnitude expected. Typical values reported for TiC, TiN, NbC and NbN [26,27] were 26.8 [28], 19.0 [29], 22.0 [30], and 12.5 [31] GPa, respectively. Currently, few studies have been published on the SPS of these complex ceramics, and the only hardness value reported for a ternary compound is 18.2 GPa for TiC_xN_{1-x} [9].

These values are in agreement with the present results for the $TiC_{0.5}N_{0.5}$ and $NbC_{0.5}N_{0.5}$ end-members of the $Ti_yNb_{1-y}C_xN_{1-x}$ solid solution, however, the hardness of the quaternary ceramics (specimens C-T7N3, C-T5N5, and C-T3N7) is noticeably higher. In general, the hardness of a multicomponent system has been described as the arithmetic average of the hardness of the constituent phases, and it is expected to be somewhere in between the minimum and maximum values of the components. Usually,

predicting the hardness of solid solution materials also assumes this multicomponent model, but sometimes, as in the present case, it was found that the hardness exceeds significantly that given by the rule of mixtures [32-34]. Moreover, Königshofer et al. [35] have shown the existence of clear maxima of the hardness in quaternary transition metal carbonitride systems with changing composition. The higher density and the lower grain size (Figure 5) observed in the quaternary ceramics may also contribute to the enhanced hardness.

The experimentally obtained values of K_{IC} for the studied samples are shown in Table 3, where it can be observed that they lie in the range of ceramic materials and are in agreement with data reported for similar materials [36,37]. However, the quaternary ceramics have shown lower toughness values than the ternary end-member ceramics. In Figure 5 it can be appreciated that the $Ti_{0.7}Nb_{0.3}C_{0.5}N_{0.5}$ (C-T7N3 specimen) presented the finest microstructure compared to the other quaternary compositions. Moreover, the grains are of various diameters between 1 and 2 μm with a relative homogenous distribution around 1 μm. On the other hand, $Ti_{0.5}Nb_{0.5}C_{0.5}N_{0.5}$ (C-T5N5) and $Ti_{0.3}Nb_{0.7}C_{0.5}N_{0.5}$ (C-T3N7) ceramics presented a bimodal microstructure with grains smaller than 0.5 μm and greater than 3 μm. Traditional reinforcement mechanisms such as crack bridging are limited due to the small grain size observed in the composites.

In the case of ternary end-member ceramics, the grain size was much larger, especially for $TiC_{0.5}N_{0.5}$ (C-T1 specimen), which showed a clear intergranular fracture. The C-N1 specimen corresponding to the $NbC_{0.5}N_{0.5}$ ceramic showed the highest fracture toughness combining both fracture modes intragranular and transgranular, as it can be clearly seen in Figure 5e.

In summary, the quaternary titanium-niobium carbonitride ($Ti_yNb_{1-y}C_xN_{1-x}$) ceramics with different *y* values obtained by a one step innovative MSR process showed after sintering by SPS technique complete densification and high nanomechanical properties compared with ternary system obtained by same conditions. An optimal combination of hardness and toughness was obtained for $Ti_{0.7}Nb_{0.3}C_{0.5}N_{0.5}$ ceramic, with values of 22.2 GPa and 3.5 MPa $m^{1/2}$, respectively. A maximum hardness value of 26.0 GPa was observed for the $Ti_{0.3}Nb_{0.7}C_{0.5}N_{0.5}$ composition.

3.3. Tribological behavior

Figure 6 shows the friction coefficient and wear rate of $Ti_yNb_{1-y}C_xN_{1-x}$ ceramics sliding against Al_2O_3 at room temperature. It can be observed that bulk $Ti_yNb_{1-y}C_xN_{1-x}$ ceramics have high friction coefficients (>0.60). In particular, the quaternary ceramics exhibit friction coefficient values above 0.70. These high values are not surprising, taking into account the severity of the test due to the absence of lubrification.

On the other hand, Figure 6 also shows the general tendency of a significant reduction in the wear rate of $Ti_yNb_{1-y}C_xN_{1-x}$ ceramics with increasing Nb content, except the C-N1 specimen that fails this trend due to its lower hardness. The $Ti_{0.3}Nb_{0.7}C_{0.5}N_{0.5}$ composition (specimen C-T3N7) showed negligible wear volume and exhibited extremely low wear rate with a value of 8×10^{-8} mm^3 m^{-1} N^{-1}. Comparing Figures 4 and 6, a first approximation would be that the higher the hardness, the wear resistance is enhanced. This behavior agrees with the Archard's wear equation that predicts that the material loss is inversely proportional to the bulk hardness. However, in view of wear rate of C-N1 specimen, wear rate not only depends on hardness, but

also toughness is involved. Although this specimen has the lowest hardness, its improved toughness allows reducing fragmentation, one of the phenomena responsible for wear, leading to a lower value of wear than expected from its hardness. As mentioned above, there is not tribological study on $Ti_yNb_{1-y}C_xN_{1-x}$ bulk materials; nevertheless, the tribological behaviors of the examined specimens are consistent with studies on related bulk ceramics, such as TiN and TiCN [38-40].

Figure 7 shows the SEM images of the worn surfaces of $Ti_yNb_{1-y}C_xN_{1-x}$ ceramics sliding against Al_2O_3. The worn surface of C-T7N3 specimen, Figure 7a, is characterized mainly by relatively smooth areas and fractured areas. In this figure, two different layers are observed because the large fragments that remain on the wear track are reduced to fine debris by continuing fracture and, subsequently, this fine debris is compacted on the worn surface. The wear mechanism in C-T5N5 ceramic, Figure 7b, is primarily determined by brittle fracture and grain pullout. In the worn surface of C-T3N7 ceramic, Figure 7c, a few cracks are found in the surface, due to mechanical polishing and plastic deformation of the compacted wear debris. Fracture combined with delamination was the major wear mechanisms in the C-T1 material. The worn surface of this material shows a major damage with a higher wear rate compared with the others materials. Finally, C-N1 specimen shows very smooth worn surfaces with lower damage as microfracture, probably due to its higher toughness.

Generally, the wear of ceramics under dry sliding is determined by mechanically dominated wear mechanisms (abrasive wear, grain boundary fatigue, delamination) [41,42] due to their intrinsic brittle nature. However, some of the $Ti_yNb_{1-y}C_xN_{1-x}$ ceramics have shown interesting features in the tribological behavior under dry sliding

contacts, mainly a reduced mechanical wear with very low wear rates of $< 1\times10^{-6}$ mm^3 m^{-1} N^{-1} due to a good combination of toughness and hardness.

4. Conclusions

Dense monolithic $Ti_yNb_{1-y}C_xN_{1-x}$ ceramics were fabricated successfully by spark plasma sintering at 1500 ºC in vacuum from solid solution synthesized by a mechanically-induced self-sustaining process. The influence of Nb and Ti content on the microstructure and mechanical properties has been clearly observed. The presence of Nb in the quaternary ceramic leads to an increase of hardness but to a decrease of toughness. $Ti_{0.3}Nb_{0.7}C_{0.5}N_{0.5}$ composition exhibits the finest microstructure and the best nanomechanical properties, hardness of 26.0 GPa and Young's module of 400 GPa. The ceramic materials containing Nb also possess interesting wear properties at dry sliding conditions, and higher wear resistances are obtained for harder ceramic samples containing higher niobium contents.

Acknowledgements

The authors would like to thank Dr. Emilio Rayón for performing the nanoindentation analysis in the Materials Technology institute (ITM) of the Polytechnic University of Valencia and to acknowledge the financial support received from Spanish Ministry of Science and Innovation for FPI grant (MAT2006-01783). This work was supported by the Spanish government under grant (MAT2010-17046), which is financed in part by the European Regional Development Fund of 2007-2013. E. Chicardi was supported by CSIC through a JAE-Pre grant, which is financed in part by the European Social Fund (ESF).

References

[1] L. E. Toth, "Transition metal carbides and nitrides", New York, Academic Press, 1971.

[2] H. Do, "Advanced TiC and TiN based cermets", in: Almond EA, Brookes CA, Warren R (Eds.). Science of hard materials. Bristol: Adam Hilger. pp. 489-521, 1986.

[3] D. Mari, S. Bolognini, G. Feusier, T. Cutard, T. Viatte, W. Benoit, Int. J. Refract. Met. Hard Mater. 21 (2003) 47-53.

[4] P. Ettmayer, H. Kolaska, W. Lengauer, K. Dreyer, Int. J. Refract. Met. Hard Mater. 13 (1995) 343-351.

[5] T. Gibas, J. Walter, L. Jaworska, B. Krolicka, J. Mater. Process. Technol. 64 (1997) 133-140.

[6] L. Chen, W. Lengauer, K. Dreyer, Int. J. Refract. Met. Hard. Mater. 18 (2000) 153-161.

[7] F. Monteverde, V. Medri, A. Bellosi, J. Eur. Ceram. Soc. 22 (2002) 2587-2593.

[8] P. Angerer, L. G. Yu, K. A. Khor, G. Korb, I. Zalite, J. Eur. Ceram. Soc. 25 (2005) 1919-1927.

[9] A. Borrell, A. Fernández, R. Torrecillas, J.M. Córdoba, M.A. Avilés, F.J. Gotor, J. Am. Ceram. Soc. 93 (2010) 2252-2256.

[10] P. Ettmayer, H. Kolaska, W. Lengauer, K. Dreyer, Int. J. Refract. Met. Hard Mater. 13 (1995) 343-351.

[11] M.G. Gee, M.J. Reece, B. Roebuck, J. Hard Mater. 3 (1992) 119-142.

[12] H. Takaoka, "Carbonitride-type cermet cutting tool having excellent wear resistance", US Patent 5710383 (1998).

[13] A. Gomathi, Mater. Res. Bull. 42 (2007) 870-874.

[14] J. Grins, J. Eur. Ceram. Soc. 17 (1997) 1819-1824.

[15] K.H. Lee, C.H. Park, Y.S. Yoon, J.J. Lee, Thin Solid Films 385 (2001) 167-173.

[16] J.M. Córdoba, M.J. Sayagués, M.D. Alcalá, F.J. Gotor, J. Mater. Chem. 17 (2007) 650-653.

[17] J.M. Córdoba, M.A. Avilés, M.J. Sayagués, M.D. Alcalá, F.J. Gotor, J. Alloy Compd. 482 (2009) 349-355.

[18] J. Rodriguez-Carvajal, "FullProf.2k Rietveld, Profile Matching & Integrated Intensities Refinement of X-ray and/ or Neutron Data (Powder and/or Single-Crystal)", Laboratoire Léon Brillouin, Centre d'Etudes de Saclay, Gif-sur-Yvette Cedex, France, 2006.

[19] W.C. Oliver, G.M. Pharr, J. Mater. Res. **7** (1992) 1564-1583.

[20] I. Pollini, A. Mosser, J.C. Parlebas, Phys. Rep. 355 (2001) 1-72.

[21] T.H. Fang, S.R Jian, D.S. Chuu, Appl. Surf. Sci. 228 (2004) 365-372.

[22] D.K. Shetty, I.G. Wrigth, P.N. Mincer, A.H. Clauer, Mater. Sci. 20 (1985) 1873-1882.

[23] A. Boultif, D. Louer, J. Appl. Cryst. 37 (2004) 724-731.

[24] J.M. Córdoba, M.J. Sayagués, M.D. Alcalá, F.J. Gotor, J. Am. Ceram. Soc. 88 (2005) 1760-1764.

[25] J.M. Córdoba, M.J. Sayagués, M.D. Alcalá, F.J. Gotor, J. Am. Ceram. Soc. 90 (2007) 381-387.

[26] H.O. Pierson, Handbook of refractory carbides and nitrides, Noyes Publications, Westwood, New Jersey, USA, 1996.

[27] H. Holleck, J. Vac. Sci. Technol. A. 4 (1986) 2661-2669.

[28] H. Abderrazak, F. Schoenstein, M. Abdellaoui, N. Jouini, Int. J. Refract. Met. Hard Mater. 29 (2011) 170-176.

[29] Sh. Kawano, J. Takahashi, Sh. Shimada, J. Am. Ceram. Soc. 86 (2003) 1609-1611.

[30] B.R. Kim, K.D. Woo, J.K. Yoon, J.M. Doh, I. Shon, J. Alloys Comp. 481 (2009) 573-576.

[31] S. Ran, L. Gao, J. Am. Ceram. Soc. 91 (2008) 599-602.

[32] C. Muroz, Am. Ceram. Soc. Bull. 73 (1994) 78-81.

[33] V. Richter, A. Beger, J. Drobniewski, I. Endler, E. Wolf, Mat. Sci. Eng. A. 209 (1996) 353-357.

[34] Q.M. Hu, K. Kadas, S. Hogmark, R. Yang, B. Johansson, L. Vitos, Appl. Phys. Lett. 91 (2007) 121918.

[35] R. Königshofer, A. Liersch, W. Lengauer, T. Koch, M. Scheerer, W. Hohenauer, "Solid-state properties of binary, ternary and quaternary transition metal carbonitrides", Proceedings of PM World Conference (2004).

[36] O. Zgalat-Lozynskyy, M. Herrmann, A. Ragulya, J. Eur. Ceram. Soc. 31 (2011) 809-813.

[37] R. Vaßen, D. Stover, Mat. Sci. Eng. A. 301 (2001) 59-68.

[38] J. Russias, S. Cardinal, J. Fontaine, G. Fantozzi, C. Esnouf, K. Bienvenu, Int. J. Refract. Met. Hard Mater. 23 (2005) 344-349.

[39] J. Meng, J. Lu, J. Wang, S. Yang, Mater. Sci. Eng. A. 418 (2006) 68-76.

[40] T. Polcar, R. Novák, P. Siroký, Wear 260 (2006) 40-49.

[41] S.M. Hsu, M. Shen, Wear 256 (2004) 867-878.

[42] A. Skopp, M. Woydt, K. Habig, Wear 181-183 (1995) 571-580.

Sample	Initial powder mixture Ti/Nb/C atomic ratio	t_{ig} (min)	Lattice parameter, a (Å)
P-T1	1/0/0.5	47	4.2998
P-T7N3	0.7/0.3/0.5	39	4.3348
P-T5N5	0.5/0.5/0.5	39.5	4.3579
P-T3N7	0.3/0.7/0.5	44.5	4.3871
P-N1	0/1/0.5	51	4.4232

Table 1. Mixtures submitted to milling, the ignition time, t_{ig}, of the MSR process, and the lattice parameter, *a*, of the obtained $Ti_yNb_{1-y}C_xN_{1-x}$ solid solution.

Specimen	Ceramic product	Density (g cm^{-3})	Relative density (%)	Lattice parameter, *a* (Å)
C-T1	$TiC_{0.5}N_{0.5}$	4.73 ± 0.01	98.7	4.2938
C-T7N3	$Ti_{0.7}Nb_{0.3}C_{0.5}N_{0.5}$	5.81 ± 0.01	99.2	4.3312
C-T5N5	$Ti_{0.5}Nb_{0.5}C_{0.5}N_{0.5}$	6.51 ± 0.01	99.2	4.3671
C-T3N7	$Ti_{0.3}Nb_{0.7}C_{0.5}N_{0.5}$	7.01 ± 0.01	99.3	4.4008
C-N1	$NbC_{0.5}N_{0.5}$	7.77 ± 0.01	98.8	4.4251

Table 2. Density of ceramics sintered by SPS at 1500 ºC and 80 MPa of pressure, and lattice parameter, *a*, of the $Ti_yNb_{1-y}C_xN_{1-x}$ solid solution after sintering.

Specimen	Toughness (MPa $m^{1/2}$)
C-T1	3.49 ± 0.04
C-T7N3	3.47 ± 0.07
C-T5N5	2.37 ± 0.02
C-T3N7	2.66 ± 0.03
C-N1	4.34 ± 0.04

Table 3. Toughness of monolithic ceramics sintered by SPS.

Figure 1

Click here to download high resolution image

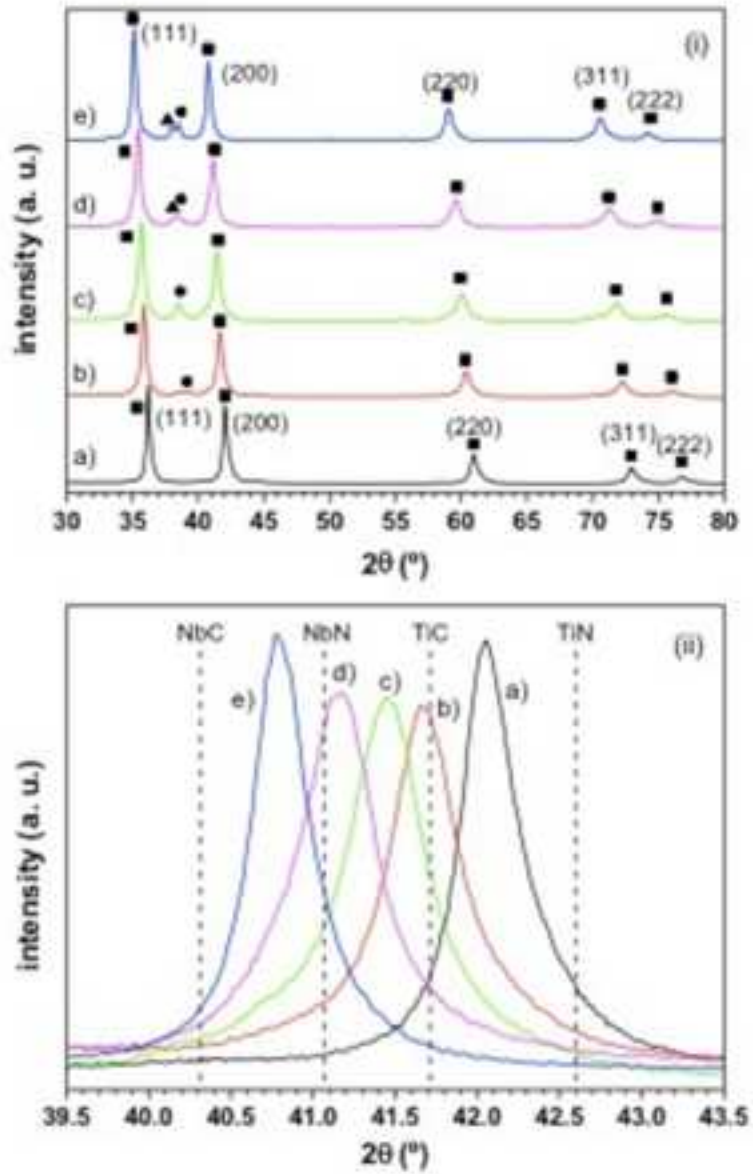

Figure 1. (i) X-ray powder diffraction diagrams of products obtained after the MSR process for samples: a) P-T1, b) P-T7N3, c) P-T5N5, d) P-T3N7, and e) P-N1. (■) $Ti_yNb_{1-y}C_xN_{1-x}$; (●) Nb; (▲) Nb_2C. (ii) (200) reflexions of the *Fm-3m* cubic structure for the same samples. The lines indicate the position of this reflexion in the binary compounds NbC, NbN, TiC, and TiN.

Figure 2

Click here to download high resolution image

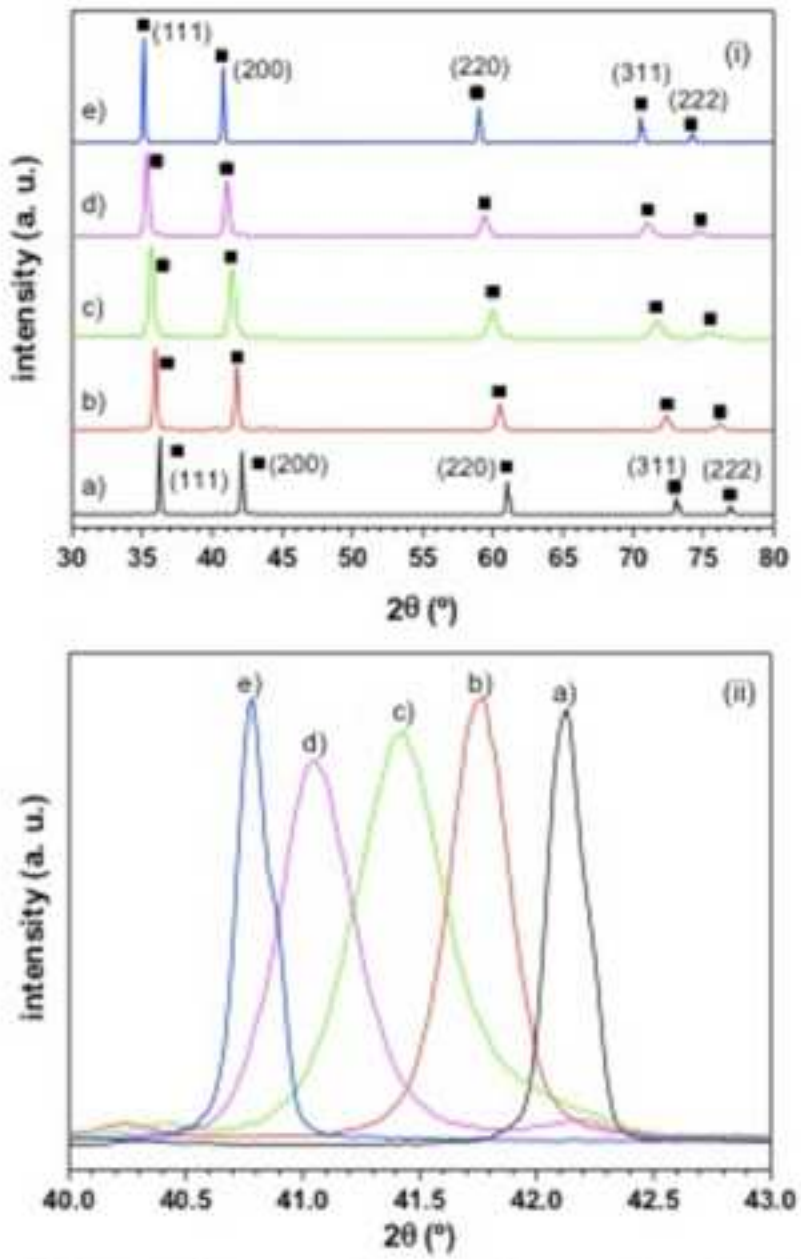

Figure 2. (i) X-ray diffraction diagrams of monolithic ceramics after the SPS process: a) C-T1, b) C-T7N3, c) C-T5N5, d) C-T3N7, and e) C-N1. (■) $Ti_yNb_{1-y}C_xN_{1-x}$. (ii) (200) reflexion of $Ti_yNb_{1-y}C_xN_{1-x}$ phase.

Figure 3
Click here to download high resolution image

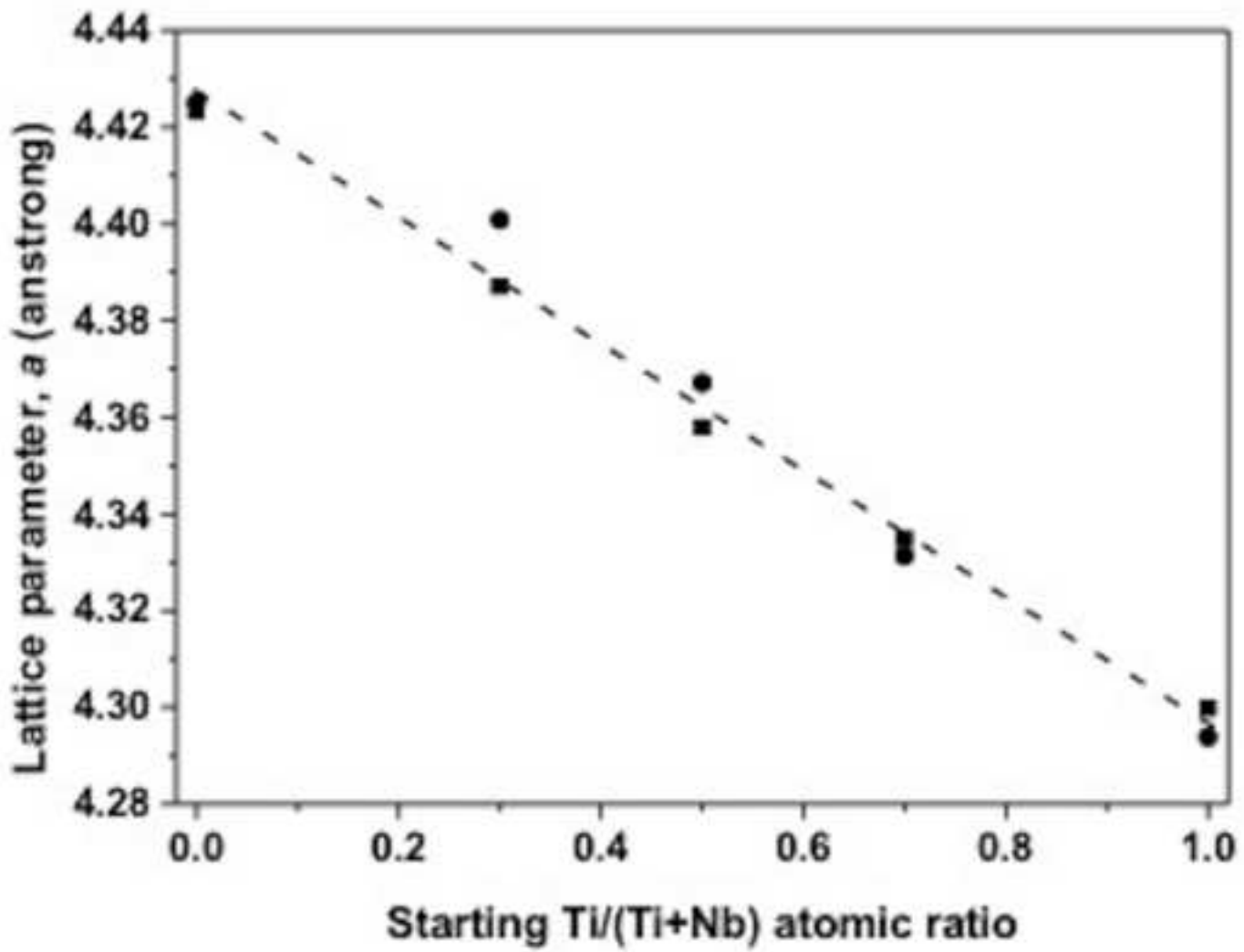

Figure 3. Lattice parameter, *a*, of the $Ti_yNb_{1-y}C_xN_{1-x}$ solid solution (■) obtained by MSR and (•) after SPS sintering as a function of the Ti/(Ti+Nb) ratio in the starting mixture submitted to milling.

Figure 4
Click here to download high resolution image

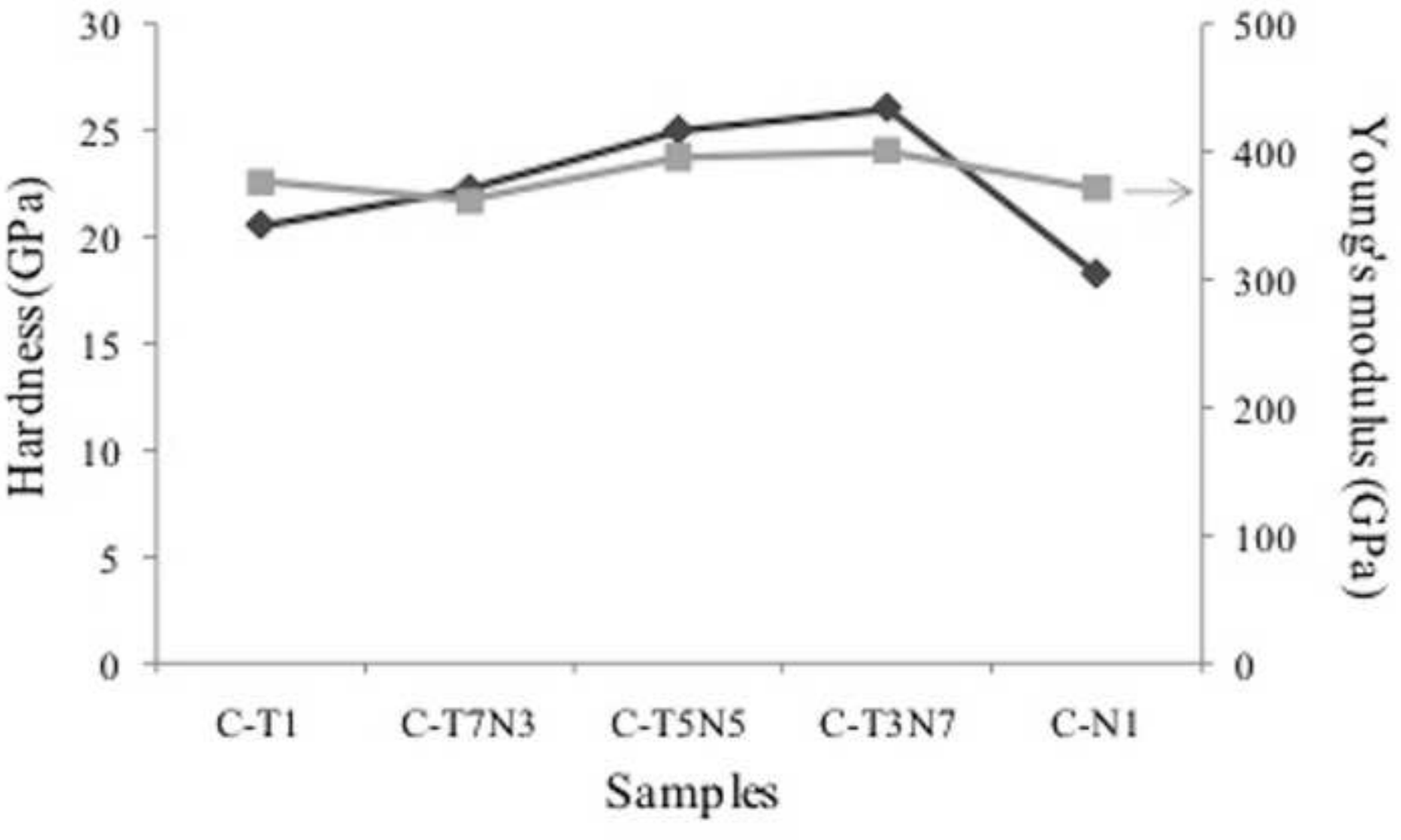

Figure 4. Nanomechanical properties of monolithic ceramics.

Figure 7
Click here to download high resolution image

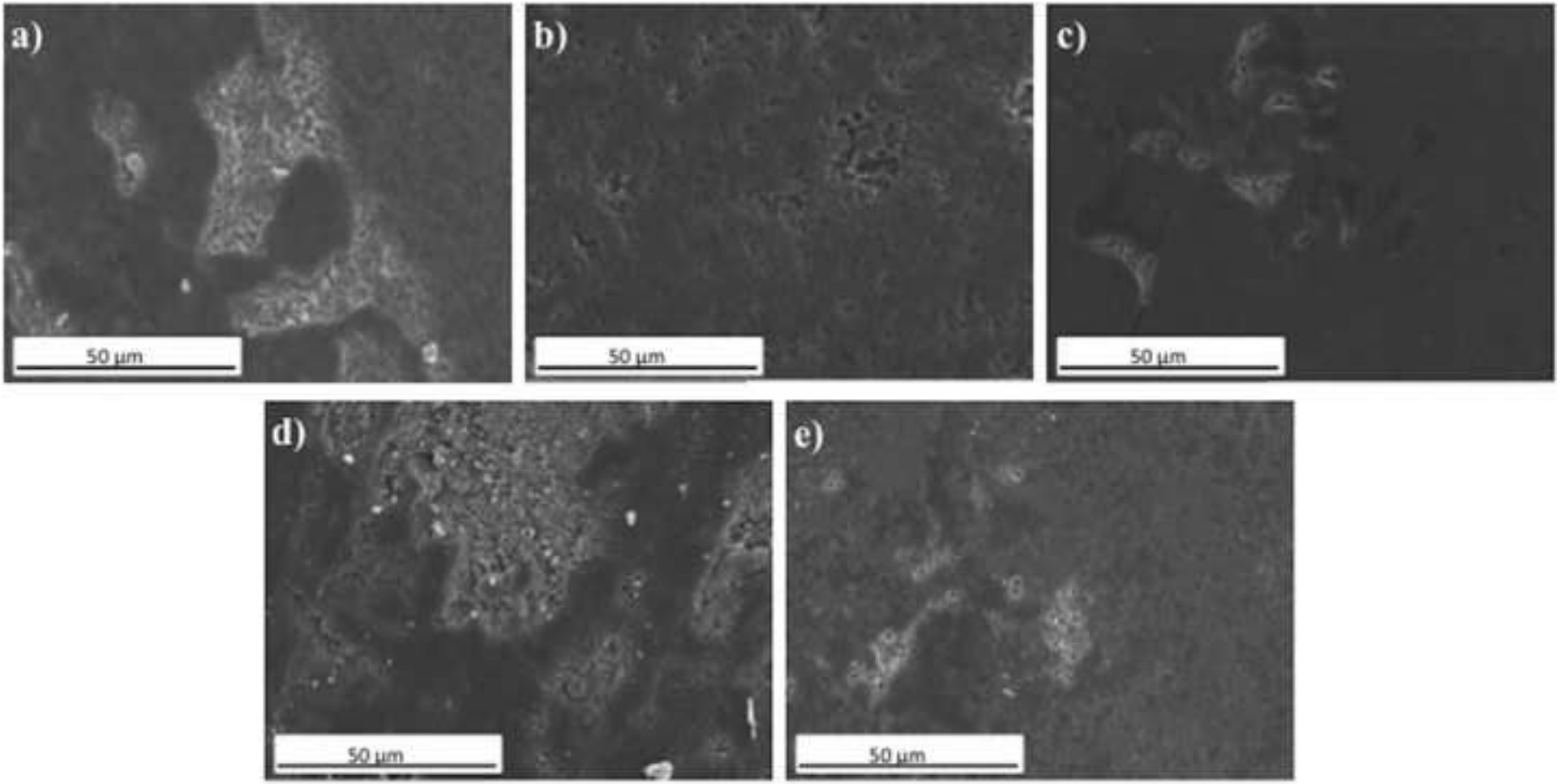

Figure 7. SEM images of worn surface of $Ti_yNb_{1-y}C_xN_{1-x}$ cermets. (a) C-T7N3, (b) C-T5N5, (c) C-T3N7, (d) C-T1, and (e) C-N1.

Figure 5
Click here to download high resolution image

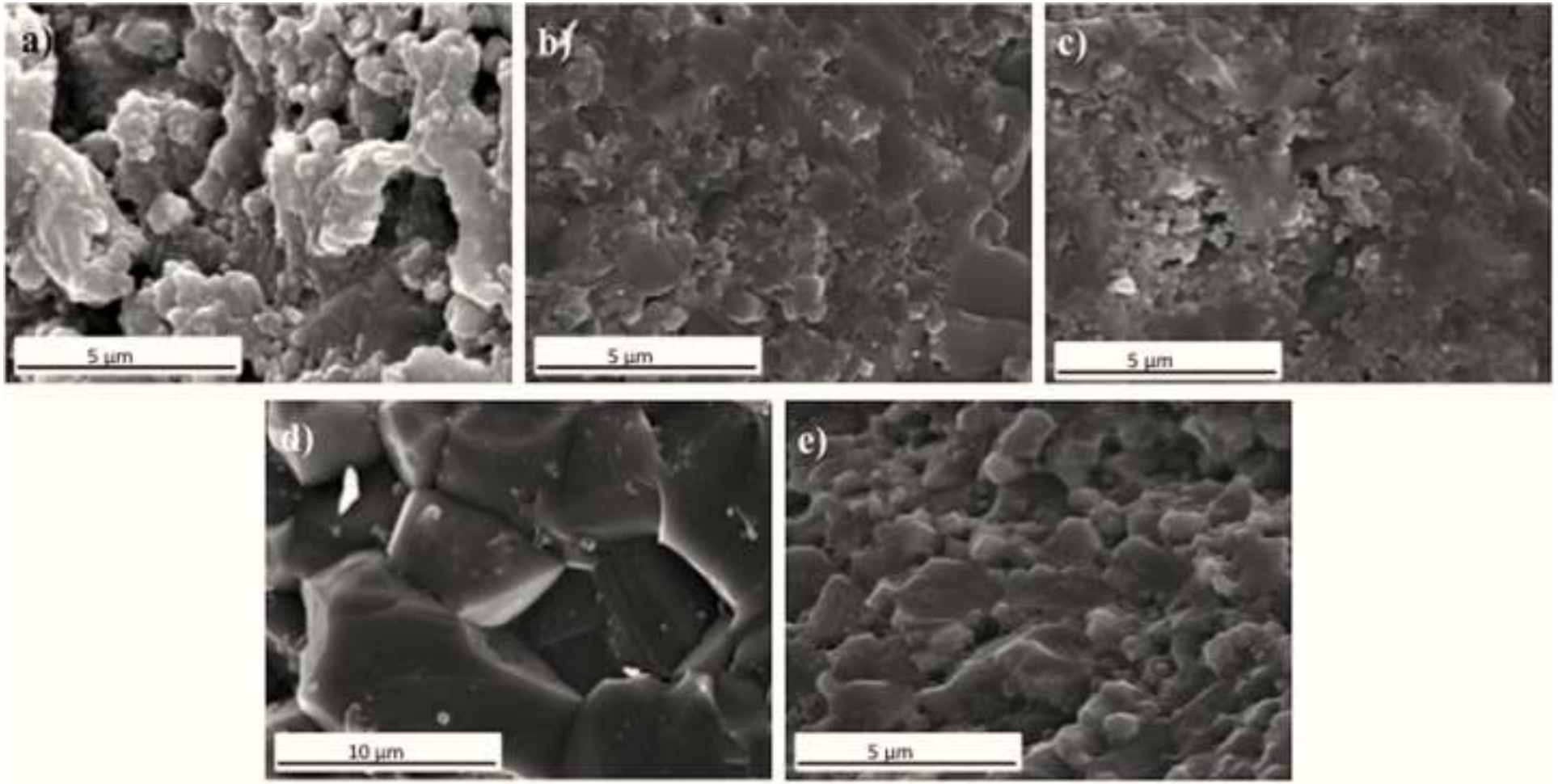

Figure 5. SEM micrographs of fracture surface of $Ti_yNb_{1-y}C_xN_{1-x}$ ceramics. (a) C-T7N3, (b) C-T5N5, (c) C-T3N7, (d) C-T1, and (e) C-N1.

Figure 6
Click here to download high resolution image

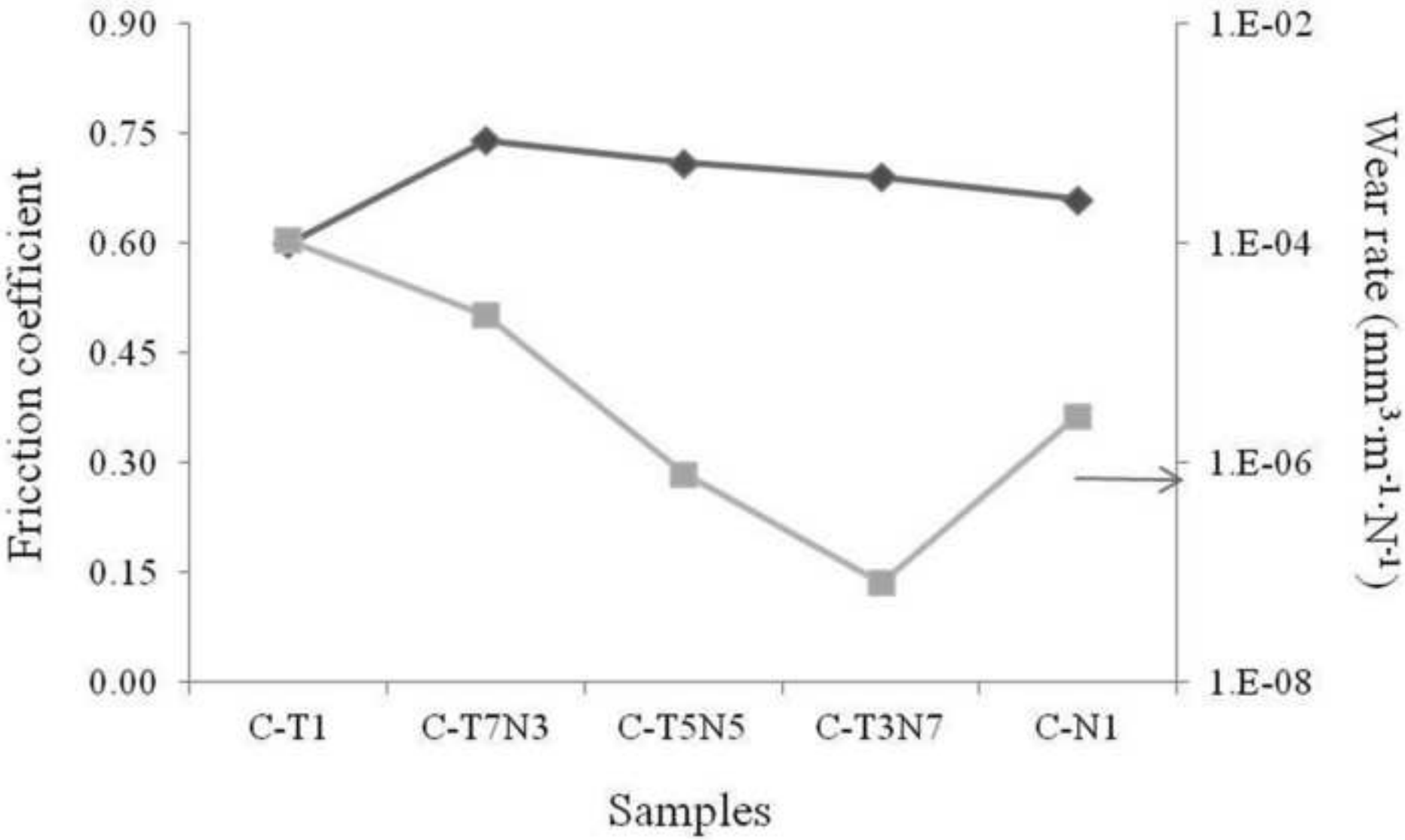

Figure 6. Friction coefficients and wear rates of $Ti_yNb_{1-y}C_xN_{1-x}$ ceramics.